Compression-compression fatigue of $Pd_{43}Ni_{10}Cu_{27}P_{20}$ metallic glass foam

Gongyao Wang,[1,a)] Marios D. Demetriou,[2] Joseph P. Schramm,[2] Peter K. Liaw,[1] and William L. Johnson[2]
[1]*Department of Materials Science and Engineering, The University of Tennessee, Knoxville, Tennessee 37996, USA*
[2]*Keck Laboratory, California Institute of Technology, Pasadena, California 91125, USA*

(Received 2 March 2010; accepted 28 May 2010; published online 20 July 2010)

Compression-compression fatigue testing of metallic-glass foam is performed. A stress-life curve is constructed, which reveals an endurance limit at a fatigue ratio of about 0.1. The origin of fatigue resistance of this foam is identified to be the tendency of intracellular struts to undergo elastic and reversible buckling, while the fatigue process is understood to advance by anelastic strut buckling leading to localized plasticity (shear banding) and ultimate strut fracture. Curves of peak and valley strain versus number of cycles coupled with plots of hysteresis loops and estimates of energy dissipation at various loading cycles confirm the four stages of foam-fatigue. © *2010 American Institute of Physics*. [doi:10.1063/1.3457221]

I. INTRODUCTION

The mechanical behavior of metallic glasses has intrigued scientists since their inception in 1960.[1] Masumoto[2] and Davis[3] were among the first scientists to study the mechanical behavior of these metal alloys. The unique features of the metallic-glass performance reported in those early investigations were universally high strength and elasticity, and a near-zero tensile ductility. These universal features were more recently attributed to an atomic structure defined by length scales on the order of several hundred atoms. Such atomic structure enables a high elastic limit but lacks microstructural mechanisms to arrest propagating plastic flow bands (shear bands).[4] Another important finding in those early studies was that unlike silicate glasses, metallic glasses demonstrate significant fracture toughness,[5–8] which for certain metallic-glass alloys approaches values typical of crystalline metals. Owing to such relatively high toughness, amorphous metals are able to undergo considerable plastic deformation in bending when sample sizes fall below a critical dimension.[9] This critical dimension is related to the maximum attainable shear in a propagating shear band,[10] which gives rise to a "plastic zone" operating ahead of a track tip. Another interesting attribute of their significant toughness and their ability to resist fracture within a finite plastic zone is their ability to attain an endurance limit upon cyclic loading (fatigue).[11,12] The fatigue-endurance capability of these materials stimulated considerable interest over the last decade, and spurred a significant number of investigations to assess their fatigue behavior.[13,14]

The plastic deformability in bending demonstrated by metallic-glass wires and plates having dimensions below the material plastic zone has inspired the development of metallic-glasses foams.[15–19] Introducing substantial porosity in a metallic glass results in a random network of cells and intracellular struts/membranes with thicknesses on the order of the plastic zone or less.[20,21] The stochastic cellular structure enables the metallic-glass foam to evade catastrophic fracture and to deform plastically to high strains attaining full densification.[17–19] When a critical threshold of randomness is attained through the introduction of porosity, the foam demonstrates an elastic behavior self-similar to the parent monolithic glass.[22] More interestingly, when the key structural scales controlling the various modes of failure of the metallic glass are matched, the foam exhibits a strength self-similar to the monolithic glass, and, consequently, emerges as one of the strongest foams of any kind.[23] Therefore, control of the various features of the cellular structure can determine the elasticity, strength, and fracture resistance of the metallic-glass foam.

Since a metallic-glass foam with adequate fracture resistance can be developed, it would be interesting to determine if such foam can attain an endurance limit upon fatigue loading. In this article, the fatigue characteristics of closed-cell metallic glass foams of varying porosity are investigated. The foam fatigue behavior is interpreted within the mechanisms governing the collapse of metallic-glass foams, and more generally within the mechanisms governing the failure of monolithic metallic glasses.

II. EXPERIMENTAL

Cylindrical closed-cell amorphous $Pd_{43}Ni_{10}Cu_{27}P_{20}$ foam samples of various porosities were prepared by the thermoplastic expansion of amorphous foam precursors. The details of the foaming method are described elsewhere.[19,20] The amorphous nature of each foam sample was verified using x-ray diffraction. The foams were sectioned with a diamond saw, and the faces were polished plane-parallel, forming cylindrical specimens with aspect ratios (height/diameter) ranging between 0.5 and 1. Short aspect ratios can be allowed in such highly porous specimens, since stress concentrations in the vicinity of pores would render the stress concentration at the specimen corners insignificant. The images of three foam specimens of varying porosity are presented in Fig. 1.

[a)]Electronic mail: gwang@utk.edu.

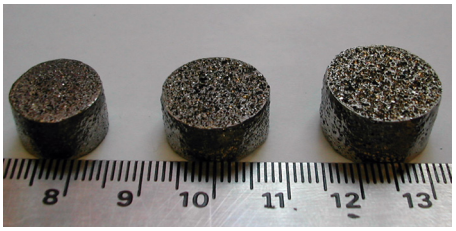

FIG. 1. (Color online) Images of three Pd-based metallic-glass foam specimens of varying porosity. The porosities (from left to right) are 70%, 81%, and 86%.

The quasi-static compressive-loading (single cycle) behavior of six foam specimens with porosities ranging between 35% and 79% was investigated, using a screw-driven Instron universal testing machine with a load capacity of 50 kN. Displacements were measured using a linear variable differential transformer. The strain rates for the quasistatic tests ranged between 10^{-3} and 10^{-4} s^{-1}. The cyclic compressive-loading behavior of ten foam specimens with porosities ranging between 41% and 81% were studied using a computer-controlled material test system servohydraulic-testing machine. Load-controlled compression-compression fatigue experiments were performed at various stress ranges with a R ratio ($R=|\sigma|_{min}/|\sigma|_{max}$, where $|\sigma|_{min}$ and $|\sigma|_{max}$ are the applied minimum and maximum stresses, respectively) of 0.1 using a sinusoidal waveform at a frequency of 10 Hz. Tungsten-carbide spacers were employed above and below the specimen. Fatigue tests were carried out until samples either failed or achieved "runout" at 10^7 cycles. An extensometer was employed to monitor strain. Scanning-electron microscopy (SEM) examinations were performed to identify fatigue and fracture mechanisms using a Leo 1526 scanning-electron microscope with the energy-dispersive spectroscopy.

III. RESULTS

The yield strengths of the six quasi-statically loaded foam specimens are presented in Table I. Typically the foam yield strength is taken to be the peak stress representing the onset of foam failure. For a metallic glass foam, the yield strength is taken to be the stress at which the first major collapse event occurs. In Fig. 2, the relative foam strengths (the foam yield strength σ_y^* normalized by the glass yield strength, σ_{ys}, of 1630 MPa) are plotted against the relative foam densities (the foam density, ρ, normalized by the glass density, ρ_s, of 9.34 g/cc). The relative foam strengths can be correlated with the relative densities through a power law, as proposed by Gibson and Ashby:[24]

$$\frac{\sigma_y^*}{\sigma_{ys}} = A\left(\frac{\rho}{\rho_s}\right)^n. \quad (1)$$

The data analysis yields $A=0.96$ and $n=2.38$, and results in a very tight fit with an R^2 value of 0.994. Such tight fit suggests that the relative strength and relative density of the present foams are strongly correlated. As such, foam yield strengths can be accurately predicted from the knowledge of foam densities (or porosities).

Owing to the wide range of foam porosity attainable by this class of foams, which can vary from as low as 10% to as high as 90%, a wide range of yield strength can be expected. According to Eq. (1), foam yield strengths can vary from as low as ~10 MPa to as high as $\sim 10^3$ MPa. In terms of fatigue performance, therefore, distinct stress-life curves should be constructed, and unique endurance limits should be established for the various levels of foam porosity. To cover such a broad porosity range, a lengthy testing process is needed, requiring tens of metallic-glass foam specimens. Alternatively, one can assume that the fatigue endurance of these foams is universally related to the relative density, as follows from the strength—relative density correlation established above [Eq. (1)]. As such, the stress amplitude applied in a cyclic-loading test normalized by the corresponding foam yield strength, can be expected to lie on a universal

TABLE I. Static and cyclic (fatigue) loading properties of amorphous Pd-based foams of various porosities.

Porosity (%)	Yield strength (MPa)	Stress amplitude (MPa)	Fatigue ratio	Cycles to failure
35.0	559.6	⋯	⋯	⋯
51.8	302.2	⋯	⋯	⋯
60.8	151.2	⋯	⋯	⋯
69.0	93.6	⋯	⋯	⋯
74.0	60.4	⋯	⋯	⋯
78.5	43.6	⋯	⋯	⋯
40.5	458.0[a]	50.9	0.11	9.2×10^6
41.0	448.9[a]	81.0	0.18	2.0×10^5
50.0	303.1[a]	68.4	0.23	3.5×10^5
53.0	261.7[a]	81.0	0.31	1.1×10^3
64.5	134.5[a]	51.4	0.38	32
64.8	131.8[a]	29.6	0.22	6.6×10^3
69.4	94.5[a]	11.8	0.12	8.6×10^6
76.5	50.5[a]	11.3	0.22	2.2×10^5
76.9	48.5[a]	5.0	0.10	$>1.0\times10^7$
81.4	29.0[a]	4.9	0.17	1.2×10^5

[a]Foam yield strength estimated using Eq. (1).

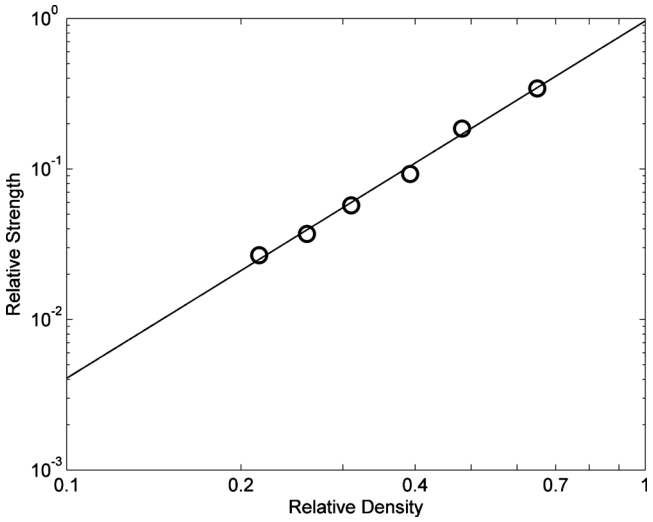

FIG. 2. Quasistatic compressive-loading data of Pd-based amorphous foams of various porosities. The relative foam strengths (foam yield strength normalized by the parent-solid yield strength of 1630 MPa) are plotted against the relative foam densities (foam density normalized by the parent-solid density of 9.34 g/cc). The solid line is a power-law fit to the data, as given by Eq. (1).

stress-life curve independent of porosity. The ratio of stress amplitude to yield strength is known as the fatigue ratio. In this study, the universal fatigue characteristics of the present metallic-glass foams are investigated by constructing a universal stress-life curve in which the fatigue ratios of foams of varying porosities are plotted against the corresponding fatigue life.

Ten metallic-glass foam specimens with porosities ranging between 41% and 81% were cyclically tested in this study. The yield strength of each foam specimen is predicted using Eq. (1). A stress amplitude that is a fraction of the foam yield strength is applied in each cyclic-loading test. The displacement limit is set to 50% of the sample height. The fatigue life, which denotes the number of cycles required to attain the set displacement limit, is determined in each test. The endurance limit in the present study is defined as the highest fatigue ratio at which the displacement limit is not reached after 10^7 cycles. The predicted yield strength, applied stress amplitude, fatigue ratio, and fatigue life for each foam specimen are tabulated in Table I.

Upon fatigue failure, the present foams tend to fragment into many small pieces. Fatigue failure at 10^7 cycles is evaded when a stress amplitude corresponding to a fatigue ratio of 0.1 is applied, thereby revealing that the foam is able to attain an endurance limit at a stress amplitude that is 10% of its yield strength. The fatigue performance of monolithic Pd-based glasses has not been studied to date. However multiple fatigue studies for the Zr-based family have been reported, and depending on the composition, loading geometry, and loading frequency, endurance limits ranging between 5% and 25% of the associated yield strengths have been reported.[13,14] Therefore, the endurance limit of the metallic-glass foam material investigated in this study appears to fall within a range representative of the fatigue-endurance limit of the parent metallic glass. By plotting the fatigue ratio versus fatigue life for the ten foam specimens, a universal stress-life curve for the foam can be constructed. The stress-life curve is shown in Fig. 3. A certain level of scatter is observed in the curve. However, the scatter is not significantly greater than that observed in stress-life curves of monolithic metallic glasses. As seen in the curve, the average fatigue life of the material increases with decreasing fatigue ratio until an endurance limit is attained, a trend consistent with stress-life curves of monolithic metallic glasses or other materials in general.[13,14]

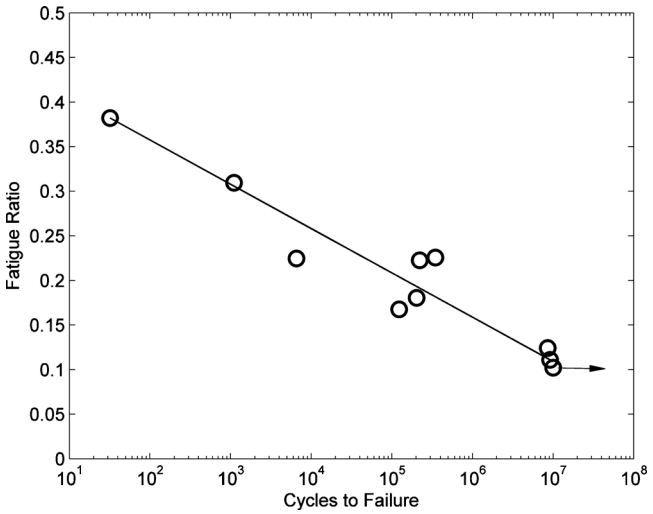

FIG. 3. Stress-life fatigue data of Pd-based amorphous foams of various porosities. The foam-fatigue ratios (applied stress amplitude normalized by the foam yield strength) are plotted against the number of cycles to failure. The solid line is a logarithmic trend-line to the data. The arrow designates the fatigue-endurance limit.

IV. MICROSCOPIC EXAMINATIONS

To analyze the local microstructure and understand the mechanism of fatigue failure in metallic-glass foams, the debris was collected and fracture surfaces were examined using SEM. Figure 4 shows the fracture surface of an individual strut in the vicinity of a fatigue-fracture surface. The fracture-surface morphology resembles typical metallic-glass fatigue-fracture features like a crack-initiation site, a crack-growth region with striations, and a fast-fracture region [Fig. 4(a)]. Interestingly, these fatigue-fracture features observed here produced by compression-compression loading are similar to fracture features produced by bending or tension loading (single cycle) of monolithic glasses.[25] In the current fatigue experiments, fatigue cracks were found to initiate typically near the thinnest section of a strut, and to propagate toward thicker strut sections [Fig. 4(b)]. Fatigue striations were observed in most of the crack-propagation region, as shown in Fig. 4(c). The crack-growth region was followed by a fast-fracture region that appears to extend toward the node. The fast-fracture region is shown to contain many irradiation ridges due to the fast and unstable advance of the fatigue crack, as seen in Fig. 4(d). The damage appears to traverse the node and spread further to neighboring cell units, as indicated by dashed arrows in Fig. 4(a), thus contributing to the development of a fatigue-fracture band that rapidly propagates across the entire structure. The cracks shown in the micrographs of Figs. 4(a)–4(d) have opened as a consequence of extensive shear band sliding. Figure 5 shows evidence of multiple extended shear bands that have propagated along a thin cell wall but failed to turn into opening cracks.

Unlike the failed specimens that suffered a significant level of structural damage due to fatigue, the 76.9%-porosity specimen that did not fail at 10^7 cycles suffered only minimal structural damage. Micrographs of the cross section of that specimen after testing are shown in Fig. 6. Even though rupture of few ultrathin cell walls is evident, thicker struts (>10 μm thick), which represent the rigid pillars of the cellular structure, appear to have suffered only minimal damage. These micrographs, therefore, suggest that metallic-glass foams enduring 10^7 loading cycles at stress amplitude as high as 10% of their yield strength are able to maintain their structural integrity.

V. DISCUSSION

Morphological irregularities of the cellular structure are known to heavily influence the buckling resistance of cellular solids.[26] Owing to the highly-stochastic cellular morphology of these foams, which involves highly-porous regions

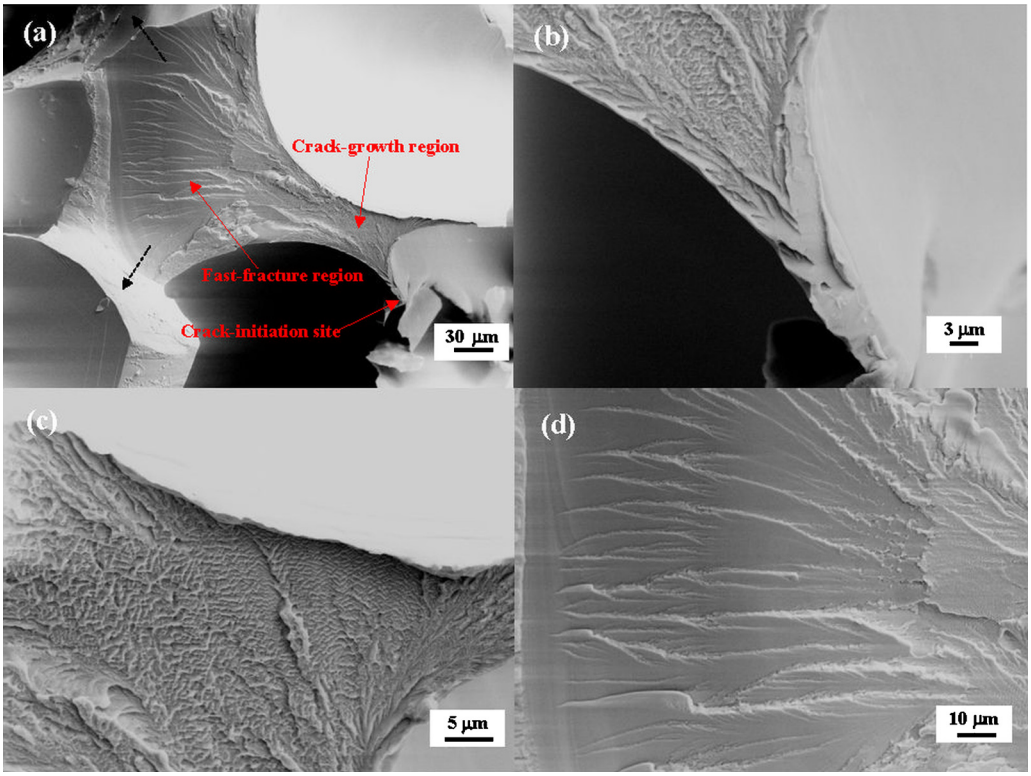

FIG. 4. (Color online) (a) Fractography of a strut in a Pd-based metallic-glass foam failed by fatigue; (b) Magnified view near the crack-initiation site; (c) Striations in the crack-propagation region; and (d) Magnified view of the fast-fracture region that traverses the node and spreads further to neighboring cell units [see dashed arrow in (a)].

with high aspect-ratio struts, and due to the high elastic limit of the metallic glass (~2%), one can assume that strut buckling should be one of the dominant mechanisms of yielding of these materials. Indeed, with the aid of the *in situ* x-ray microtomography, the dominant mechanism of yielding of these foams under static loading has been identified to be strut buckling.[22] Specifically, the highly-porous regions of the cellular structure that incorporate high-aspect-ratio struts serve as "buckling sites" where local buckling develops at relatively low strains. At higher strains, local buckling is seen to percolate, leading to the formation of deformation bands that extend across the entire structure. Buckling eventually reaches a limit of instability at some critical strain, marking the onset of plastic yielding (shear-band formation),

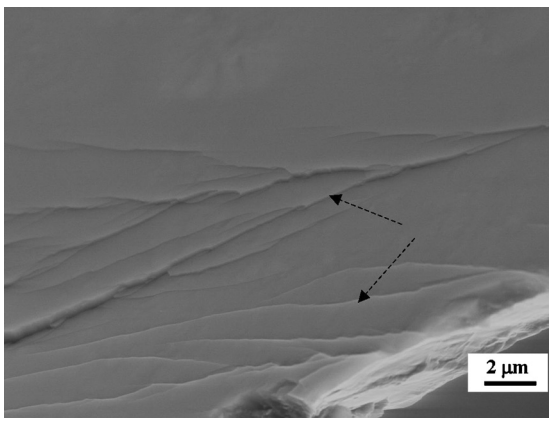

FIG. 5. Shear bands that propagated along a thin cell wall of a Pd-based metallic-glass foam specimen failed by fatigue.

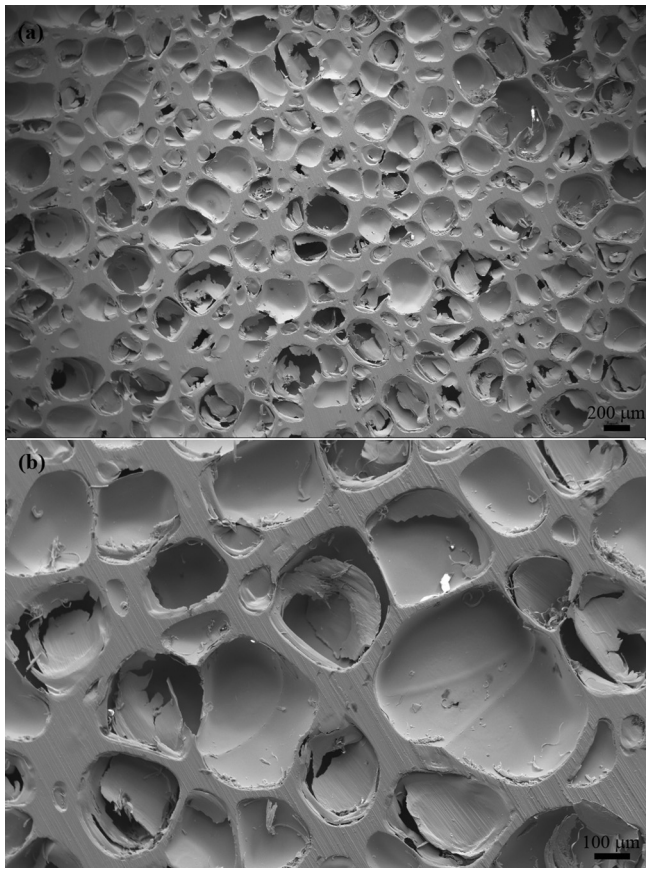

FIG. 6. Micrographs of a cellular-structure cross section of the foam specimen able to endure $>10^7$ loading cycles without fatigue failure. (a) A low magnification and (b) a high magnification.

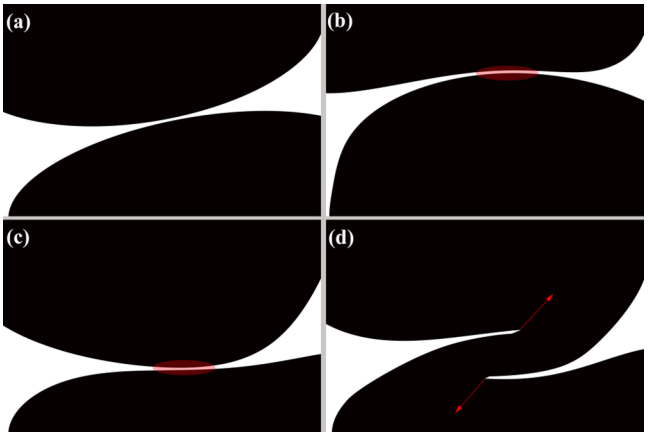

FIG. 7. (Color online) Schematic of an intracellular strut at various strain configurations. (a) Equilibrium unstrained configuration. [(b) and (c)] Distinct buckled configurations attained at different loading cycles. Ovals highlight the regions of elastic-strain energy buildup. (d) Ultimate fatigue fracture of the strut.

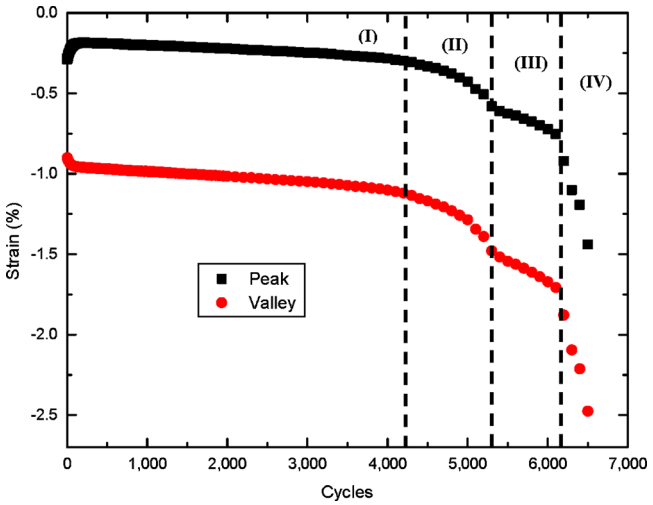

FIG. 8. (Color online) Strain-cycle curves during cyclic loading of a 50%-porosity Pd-based metallic-glass foam tested at a fatigue ratio of 0.23. Four stages are identified: (I) elastic strut buckling; (II) anelastic strut buckling; (III) plastic flow (shear banding) along buckled struts; and (IV) brittle-fracture of plastically-buckled struts.

which subsequently leads to brittle fracture (crack formation) and ultimate foam collapse. Hence, even though failure ultimately terminates by plastic yielding and brittle fracture, the yielding response is almost entirely elastic and is contributed by strut buckling. In a stress-strain curve, such elastic-yielding response is identified with an extended nonlinear stress plateau, which terminates with an abrupt stress drop that designates a collapse event.[22] An elastic-buckling yielding mechanism is also supported by the relative strength—relative density power-law correlation given in Eq. (1). According to Gibson and Ashby,[24] a power exponent of ~2 designates an elastic-buckling yielding mechanism, while the mechanisms of plastic yielding or brittle fracture are designated by a power exponent of ~1.5. The power exponent in Eq. (1) is 2.38, which is closer to that for elastic buckling than plastic yielding or brittle fracture.

The highly random polyhedral arrangement of cell faces in these cellular structures enables the nodes to have multiple degrees of freedom for elastic displacements. Under the application of strain, the degrees of freedom of the nodes give rise to several possible strut-buckling configurations. Hence, under the application of millions of loading cycles, as in fatigue loading, one can assume that buckling-prone struts could potentially attain a wide range of buckling configurations. This multiconfigurational strut buckling will result in a significant elastic-strain energy buildup in the buckling sites of the cellular structure. Most of the elastic-strain energy will accumulate in the vicinity of the thinnest strut regions, where most of the elastic strain occurs. When the elastic-strain energy buildup reaches a threshold value, one can expect the deformation within buckling sites to become anelastic and eventually plastic, leading to the formation of shear bands. Ultimately, fracture will intervene to rapidly release the stored elastic energy through the formation of cracks. This process is illustrated schematically in Fig. 7.

In order to assess the validity of the above "proposal," several experimental investigations were conducted. First, the variation in the peak and valley strain values during fatigue testing was investigated. The curves of peak and valley strain versus number of cycles are presented in Fig. 8 for the 50%-porosity foam tested at a stress amplitude that corresponds to a fatigue ratio of 0.23. As revealed in the plot of Fig. 8, the foam-fatigue process develops over four stages. The first stage which extends up to about 4000 cycles is associated with a small linear strain-increasing rate, and is identified with elastic buckling of high aspect-ratio struts confined within highly-porous regions (buckling sites) of the cellular structure. The second stage, which extends up to about 5000 cycles is associated with somewhat larger and nonlinear strain-increasing rate, and is consistent with a process of anelastic strut buckling. The boundary between the second and third stage marks the anelastic-to-plastic transition, and is associated with the onset of a buckling instability and the breakdown of elasticity. The third stage, which extends up to about 6000 cycles, is associated with large and fairly linear strain-increasing rate, and is consistent with localized plastic flow during shear-band formation. Finally, the fourth stage is associated with very large strain-increasing rate and is identified with crack initiation and growth leading to fast fracture along bands of plastically-buckled struts. The rapid intervention of fracture leads to ultimate fatigue failure of the foam specimen.

In order to further examine the above stages of foam fatigue, stress-strain hysteresis loops are considered. A stress-strain hysteresis loop provides basic information on the cyclic-loading behavior of a tested material. The measured strain represents the total strain, comprising elastic, anelastic, and plastic contributions. The progress of the hysteresis was measured at selected loading cycles to gain insight into the specific fatigue mechanism of the tested metallic-glass foams. Figure 9 shows the hysteresis loops at selected cycles for the 50%-porosity Pd-based metallic-glass foam tested at fatigue ratio of 0.23. Up to 4000 cycles, when an elastic-buckling mechanism is expected to dominate the fatigue process (see Fig. 8), a very small residual strain is recorded (~0.1%), while the width of the hysteresis loop is rather

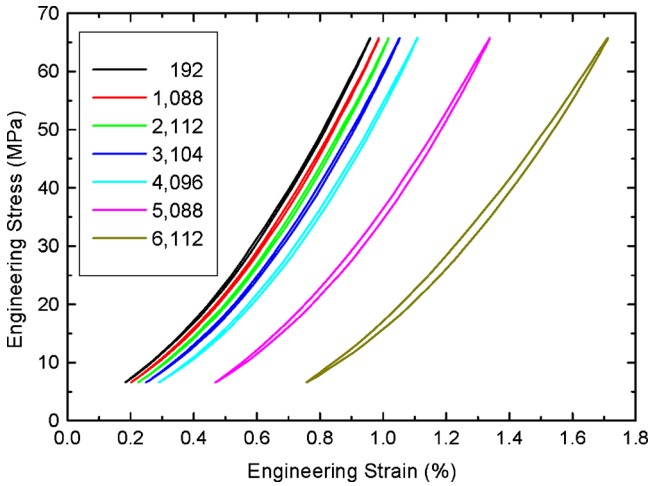

FIG. 9. (Color online) Hysteresis loops at selected cycles during cyclic loading of a 50%-porosity Pd-based metallic-glass foam tested at a fatigue ratio of 0.23.

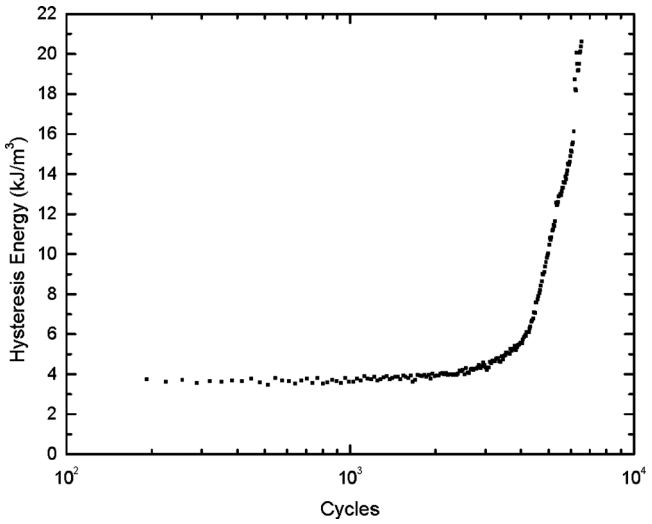

FIG. 10. Hysteresis energy vs number of cycles during cyclic loading of a 50%-porosity Pd-based metallic-glass foam tested at a fatigue ratio of 0.23.

small. At about 5000 cycles, when the fatigue process is expected to be dominated by anelastic strut buckling, the hysteresis loop becomes wider, while the residual strain grows (~0.5%), reflecting the anelastic buckling response of high-aspect-ratio struts. Finally at about 6000 cycles, when plasticity is anticipated to dominate the fatigue process, a very wide hysteresis loop is recorded, and the residual strain grows dramatically (~1%) indicating the offsets formed by multiple extended shear bands. The trends revealed by the hysteresis loop curves are consistent with those implied in curves of the peak and valley strain versus number of cycles (Fig. 8).

The increasing width of the hysteresis loops can be quantified by estimating the dissipated energy in each cycle, ΔE, defined as the area enclosed within the hysteresis loop.[27] For any given cycle, the hysteresis energy is obtained by

$$\Delta E = \int_{\varepsilon_{min}}^{\varepsilon_{max}} \sigma d\varepsilon, \tag{2}$$

where ε_{min} and ε_{max} are the minimum and maximum strains in the cycle, respectively. The energy dissipated per unit volume (in kilojoules per cubic meter) versus number of cycles for the 50%-porosity Pd-based metallic-glass foam tested at a fatigue ratio of 0.23 is presented in Fig. 10. Up to 4000 cycles, when an elastic-buckling mechanism is expected to dominate, ΔE is very small (~4 kJ/m^3) and appears to remain fairly constant with increasing the number of cycles, reflecting a roughly reversible elastic process. When 4000 cycles are exceeded, i.e., when the process becomes dominated by anelastic buckling, ΔE appears to increase modestly with increasing the number of cycles, reflecting a quasi-reversible anelastic process. Finally when 5000 cycles are exceeded, i.e., when plasticity and fracture dominate the fatigue process, ΔE increases drastically with increasing the number of cycles indicating a completely irreversible inelastic process. The trends demonstrated by the energy dissipation versus number of cycles plot are, thus, consistent with those revealed by the hysteresis loop curves (Fig. 9), as well as those implied in the curves of the peak and valley strain versus number of cycles (Fig. 8).

VI. CONCLUSIONS

Compression-compression fatigue of Pd-based metallic-glass foams of various porosities was performed. A stress-life curve based on fatigue ratio (applied stress amplitude/estimated foam yield strength) revealed an endurance limit at a fatigue ratio of about 0.1. Microscopic examinations in the vicinity of failed intracellular struts revealed typical metallic-glass fatigue-fracture features, including fatigue-crack initiation at the thinnest strut sections, a crack-growth region extending toward thicker sections covered by striations, and a fast-fracture region traversing the nodes and spreading further to neighboring cell units. Since the dominant mechanism of yielding for this class of foams has previously been identified to be elastic-strut buckling, it is understood that foam fatigue is initiated by strut buckling as well. Peak and valley strain versus number of cycles curves reveal four stages of foam fatigue: an elastic-buckling stage, an anelastic-buckling stage, a stage dominated by the plastic flow, and finally a stage dominated by brittle fracture. Plots of hysteresis loops and estimates of the energy dissipation at various loading cycles appear to confirm the four stages of foam fatigue implied by the strain-evolution curves.

ACKNOWLEDGMENTS

The present work is supported by the National Science Foundation (NSF), the Combined Research-Curriculum Development (CRCD) Program under Grant Nos. EEC-9527527 and EEC-0203415, the Integrative Graduate Education and Research Training (IGERT) Program under Grant No. DGE-9987548, the International Materials Institutes (IMI) Program under Grant No. DMR-0231320, the MRSEC Program of the National Science Foundation under Grant No. DMR-0520565, the Office of Naval Research under Grant No. N00014-07-1-1115, the Major Research Instrumentation (MRI) Program under Grant No. DMR-0421219,

the Division of Civil, Mechanical, Manufacture, and Innovation Program under Grant No. CMMI-0900271, and the Materials World Network Program under Grant No. DMR-00909037, with Ms. M. Poats, and Dr. C. J. Van Hartesveldt, Dr. D. Dutta, Dr. P. W. Jennings, Dr. L. S. Goldberg, Dr. L. Clesceri, Dr. D. Finotillo, Dr. C. Huber, Dr. C. E. Bouldin, Dr. C. V. Cooper, an Dr. A. Ardell as contract monitors.

[1]W. Klement, R. H. Willens, and P. Duwez, Nature (London) **187**, 869 (1960).
[2]T. Masumoto, Sci. Rep. Res. Inst. Tohoku Univ. A **A26**, 246 (1977).
[3]L. A. Davis, *Metallic Glasses* (ASM, Metals Park, Ohio, 1978), pp. 191–223.
[4]W. L. Johnson and K. Samwer, Phys. Rev. Lett. **95**, 195501 (2005).
[5]J. Schroers and W. L. Johnson, Phys. Rev. Lett. **93**, 255506 (2004).
[6]J. J. Lewandowski, W. H. Wang, and A. L. Greer, Philos. Mag. Lett. **85**, 77 (2005).
[7]J. J. Lewandowski, M. Shazly, and A. S. Nouri, Scr. Mater. **54**, 337 (2006).
[8]M. F. Ashby and A. L. Greer, Scr. Mater. **54**, 321 (2006).
[9]A. Inoue, M. Hagiwara, and T. Masumoto, J. Mater. Sci. **17**, 580 (1982).
[10]R. D. Conner, W. L. Johnson, N. E. Patton, and W. D. Nix, J. Appl. Phys. **94**, 904 (2003).
[11]T. Ogura, K. Fukushima, and T. Masumoto, Scr. Metall. **9**, 979 (1975).
[12]L. A. Davis, J. Mater. Sci. **11**, 711 (1976).
[13]G. Y. Wang, P. K. Liaw, and M. L. Morrison, Intermetallics **17**, 579 (2009).
[14]G. Y. Wang and P. K. Liaw, JOM **62**, 25 (2010).
[15]J. Schroers, C. Veazey, M. D. Demetriou, and W. L. Johnson, J. Appl. Phys. **96**, 7723 (2004).
[16]T. Wada and A. Inoue, Mater. Trans. **45**, 2761 (2004).
[17]A. H. Brothers and D. C. Dunand, Acta Mater. **53**, 4427 (2005).
[18]A. H. Brothers and D. C. Dunand, MRS Bull. **32**, 639 (2007).
[19]M. D. Demetriou, J. P. Schramm, C. Veazey, W. L. Johnson, J. C. Hanan, and N. B. Phelps, Appl. Phys. Lett. **91**, 161903 (2007).
[20]M. D. Demetriou, C. Veazey, J. Schroers, J. C. Hanan, and W. L. Johnson, J. Alloys Compd. **434–435**, 92 (2007).
[21]M. D. Demetriou, C. Veazey, J. Schroers, J. C. Hanan, and W. L. Johnson, Mater. Sci. Eng., A **449–451**, 863 (2007).
[22]M. D. Demetriou, J. C. Hanan, C. Veazey, M. D. Michiel, N. Lenoir, E. Üstündag, and W. L. Johnson, Adv. Mater. **19**, 1957 (2007).
[23]M. D. Demetriou, C. Veazey, J. S. Harmon, J. P. Schramm, and W. L. Johnson, Phys. Rev. Lett. **101**, 145702 (2008).
[24]L. J. Gibson and M. F. Ashby, *Cellular Solids: Structure and Properties*, 2nd ed. (Cambridge University Press, Cambridge, UK, 1997), Chap. 5.
[25]X. K. Xi, D. Q. Zhao, M. X. Pan, W. H. Wang, Y. Wu, and J. J. Lewandowski, Appl. Phys. Lett. **89**, 181911 (2006).
[26]A. G. Evans, J. W. Hutchinson, and M. F. Ashby, Prog. Mater. Sci. **43**, 171 (1998).
[27]A. Bezazi and F. Scarpa, Int. J. Fatigue **29**, 922 (2007).